Analyst

PAPER

View Article Online
View Journal | View Issue

Cite this: *Analyst*, 2023, **148**, 3559

Efficiency of direct photoinduced generation of singlet oxygen at different wavelengths, power density and exposure time of laser irradiation

Irina Makovik, [a] Andrey Vinokurov, [a] Andrey Dunaev, [a] Edik Rafailov [b] and Viktor Dremin *[a,b]

Received 14th April 2023,
Accepted 23rd June 2023

DOI: 10.1039/d3an00587a

rsc.li/analyst

This work investigates the influence of laser irradiation parameters (wavelength, power density and exposure time) on singlet oxygen ($^1O_2$) generation efficiency. Chemical trap (L-histidine) and fluorescent probe (Singlet Oxygen Sensor Green, SOSG) detection methods were used. Studies have been conducted for 1267, 1244, 1122 and 1064 nm laser wavelengths. 1267 nm had the highest efficiency of $^1O_2$ generation, but 1064 nm demonstrated almost the same efficiency. We also observed that the 1244 nm wavelength can generate some amount of $^1O_2$. It was demonstrated that laser exposure time can generate $^1O_2$ more efficiently than an increase of power. Additionally, the SOSG fluorescence intensity measurements method for acute brain slices was studied. This allowed us to evaluate the approach's potential for *in vivo* detection of $^1O_2$ concentrations.

1 Introduction

Singlet oxygen ($^1O_2$) is an electronically excited state of triplet oxygen ($^3O_2$) that is less stable than triplet oxygen in the electronic ground state and is produced by photochemical, thermal, chemical, or enzymatic activation of oxygen triplet form.[1] The reactivity of the excited state is several orders of magnitude greater than that of the triplet form of oxygen. Recently, the mechanism of direct optical excitation (photosensitiser-free) of the basic form of oxygen in the singlet state by light at specific wavelengths has been actively studied.[2]

Recent research indicates that laser-induced $^1O_2$ may be involved in physiological cellular processes and modulate the cell's redox potential.[1,3–7] Furthermore, the production of $^1O_2$ is the essential stage of photodynamic therapy (PDT) used in the treatment of cancer, bacterial infections, and some other pathologies.[8–11]

It is obvious that the potential toxicity of $^1O_2$ to pathological as well as healthy tissues requires determining the optimal dose of irradiation that provides the desired physiological action of $^1O_2$ with the minimum possible side effects.[12] This is especially important for the direct optical generation of $^1O_2$, which is characterised by less selectivity due to the absence of a photosensitiser selective accumulation in exact tissue (for example, in a tumour).[1,13]

The determination of the optimal dose requires an appropriate experimental model and method for the detection and quantitative analysis of $^1O_2$. Considerable difficulty is associated with the peculiarities of the model systems used, in which the dose required to achieve the same result may differ significantly. Therefore, it is known that the threshold of the $^1O_2$ concentration leading to the cancer cells death *in vivo* is significantly lower than *in vitro*.[14]

Obviously, the physiological effect of $^1O_2$ is determined not only by the rate of its production or concentration but also by the rate of diffusion and further conversion, including the transition to a stable triplet state. The change in the balance between these processes causes differences in the $^1O_2$ lifetime, which significantly depends on the physicochemical properties of the system and ranges from 4 μs to 700 μs.[15–17] At the same time, the efficiency of conversion of generated $^1O_2$ in biological processes will depend on the slowest stage (rate-limiting stage). In the case where the $^1O_2$ formation rate is drastically higher, one can expect that a significant part of the $^1O_2$ returns to a stable triplet state. In the case of comparable rates of $^1O_2$ production and conversion, the efficiency of the $^1O_2$ usage can be significantly higher.

The available information suggests that the method of achieving the irradiation dose, including the power and duration of the irradiation, may affect the nature and magnitude of the $^1O_2$ physiological effect in the systems of direct laser-induced $^1O_2$ production. For example, the positive role of

[a]*Research & Development Center of Biomedical Photonics, Orel State University, Orel, 302026, Russia. E-mail: viktor.dremin@bmecenter.ru*
[b]*College of Engineering and Physical Sciences, Aston University, Birmingham, B4 7ET, UK*

irradiation with a wavelength near 1270 nm in suppressing cancer cells was demonstrated.[18,19] However, in the study of Novikova *et al.*, there was no significant increase in the formation of other reactive oxygen species (ROS) or development of oxidative stress signs, while a significant acceleration of dihydroethidium oxidation both directly during and after irradiation was demonstrated by Semyachkina-Glushkovskaya *et al.* It is important to note the difference in irradiation dose used in these studies – 200 J cm^{-2} and 47.7 J cm^{-2} in ref. 18 and 19 respectively. Due to the lower exposure time in ref. 18, the higher laser power was used. It was very important that the conclusion about the influence of $^1O_2$ on biological processes was made on the basis of indirect data without simultaneous detection and quantitative analysis of $^1O_2$.

Therefore, along with the development of a methodology for the use of $^1O_2$ for therapeutic purposes, an important task was the search for the dependency between irradiation dose and $^1O_2$ usage efficiency for determination of the optimal conditions of direct laser-induced $^1O_2$ exciting.

Along with this, sensitive and selective methods are needed to detect concentrations of $^1O_2$. Although significant progress has been made in understanding the behaviour and biological effects of certain types of ROS (including $^1O_2$), their low concentration, high reactivity, and high kinetics make their selective detection difficult, especially *in vivo*. Recently, there have been considerable research efforts in the development of $^1O_2$ detection and quantification methods.[20–22] Electron paramagnetic resonance spectroscopy using spin traps,[23–25] luminescence at 1270 nm,[26,27] chemical trapping[28,29] and fluorescence detection using highly selective sensors (fluorescent and chemiluminescent probes)[20,30] are used to solve this task. Most of the presented methods allow not only to detect $^1O_2$ but also to determine its amount.

Thus, the assessment of the influence of the excited laser parameters (namely power and exposure of laser irradiation, as well as wavelength) for the production of $^1O_2$ remains an unsolved problem. In this work, we tried to study this issue and further evaluate the possibilities of some approaches for *in vitro* and *in vivo* detection of $^1O_2$.

2 Materials and methods

The basic triplet state of oxygen has several absorption bands in the infrared and visible regions (optical range between 1300 nm and 390 nm), at which $^1O_2$ can be produced.[31] Fig. 1 shows the absorption spectrum of oxygen dimols (dimers) in a gas compressed to 150 atm.[32,33] As a paramagnetic compound, $^3O_2$ is characterised by the rearrangement of the electron spin and orbital filling under the influence of radiation. When one orbital is filled with a pair of electrons with unidirectional spins, $^3O_2$ passes to the first excited level ($^1\Delta_g$). The condition when two electrons occupy different orbitals and have opposite electron spins corresponds to the second excited level ($^1\sum_g^+$).[34]

In this work, laser wavelengths of 1267 nm, 1244 nm, 1122 nm and 1064 nm were studied (see Fig. 1). Laser

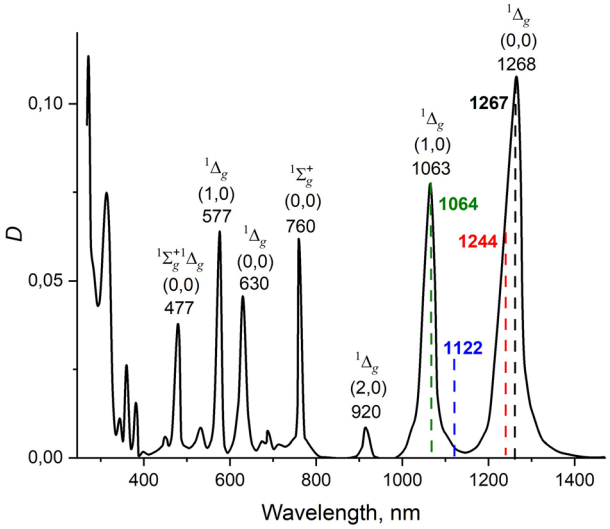

Fig. 1 Absorption spectrum of oxygen dimols (dimers) in a gas compressed to 150 atm. The graph also presents some of the main electronic transitions. Adopted from ref. 1, 32 and 35. *D* is optical density, $^1\sum_g^+$, $^1\Delta_g$ are the two lowest electronic excited states of molecular oxygen (vibrational sublevels are indicated in parentheses).

irradiations of 1244 nm and 1122 nm were used as a reference. Fig. 1 shows that 1122 nm is practically not absorbed by molecular oxygen. Although Fig. 1 also shows that 1244 nm coincides with one of the absorption lines, a similar wavelength was used in previous studies as a control.[33]

CW laser diodes SM-1267-PM-500, SM-1244-PM-500, LD-1122-PM-370, SM-1064-PM-500 (Innolume GmbH, Germany) were used as sources of laser irradiation. Laser diode driver SF8150-ZIF14 (Maiman Electronics LLC, Russia) was used to control. Laser irradiation from the source to the study object was delivered using a specially manufactured quartz fibre-optic cable. The cable provided irradiation transmission with minimal signal attenuation in the 400–2000 nm spectral range and had a numeric aperture (NA) of 0.22. The diameter of the laser beam remained fixed due to the use of an F280FC-C collimator (Thorlabs Inc., USA) and amounted to 3.4 mm.

2.1 $^1O_2$ detection using the polarographic method

As the first analyzed approach, the polarographic method using the Oxytherm+R respirometer (Hansatech Instruments, UK) with chemical trapping was considered. L-Histidine was used as a "chemical trap" in this study. Histidine reacts with $^1O_2$ to form an intermediate product, a transannular peroxide, which then rearranges or decomposes into a final oxygenation product.[28] Thus, it makes possible the polarographic measurements of the decrease in dissolved oxygen concentration. During the experiment, the level of dissolved oxygen in ddH_2O or 5 mM L-histidine solution in ddH_2O was measured. ddH_2O was used as the simplest medium to exclude the possible influence of components which can bind $^1O_2$ like L-histidine as a chemical trap. During the studies, the temperature in the

measuring chamber was 26 °C, solution volume was 750 μL. The choice of this temperature value is due to the need to ensure the similarity of the temperature conditions during experimental studies using different approaches and to compare of their results. The laser irradiation was delivered through the glass wall of the measuring chamber.

2.2 $^1O_2$ detection in solution with application of singlet oxygen sensor green

The second approach analysed was fluorescence intensity measurements with Singlet Oxygen Sensor Green (SOSG) (Invitrogen, USA). SOSG was previously characterised as a sensitive and specific probe for $^1O_2$.[36] This probe initially has a weak blue fluorescence but transforms into a form with intense green fluorescence after selective interaction with $^1O_2$.[30] The SOSG concentration in the measuring chamber during the experiments was 5 μM. Measurements were made using a Zeiss LSM 900 microscope (Carl Zeiss AG, Germany) with a 10× objective. To excite the fluorescence of the indicator, a laser with a wavelength of 488 nm and a power of 0.1% of the maximum was used. The use of laser irradiation with the parameters indicated for excitation of SOSG allowed minimising the probability of self-activation[21,37] and initiation of a self-propagating $^1O_2$ cycle once SOSG is activated.[30] The delivery of laser irradiation during the experiments was carried out from the opposite side of the microscope objective.

2.3 $^1O_2$ detection in acute brain slices with application of singlet oxygen sensor green

Additionally, the possibility of using SOSG for the detection of ^1O in acute brain slices was studied. Acute brain slices were prepared according to ref. 38 and 39. After rat decapitation, the brain was extracted and removed into a cold Hanks' Balanced Salt Solution (HBSS) (pH 7.4/4 °C) with subsequent preparation into slices with a thickness of 300–500 μm. According to the data,[40] SOSG could bind to proteins and penetrate into cells. The slices were kept in a cold HBSS with slight oxygenation. Before the experiments, the slices were moved into HBSS (pH 7.4/37 °C) with 5 μM SOSG and 0.005% pluronic acid to improve the penetrating properties of SOSG for at least 30 min.

The modified imaging setup presented in the work[41] was used for acute brain slice imaging. The setup included a Mitutoyo M Plan APO 5× planar apochromatic lens (Thorlabs, Inc. USA), AC254-050 achromatic doublet (Thorlabs, Inc. USA) and 340M-USB fast frame rate monochrome scientific CCD camera (Thorlabs, Inc. USA) with the FELHO500 (Thorlabs, Inc. USA) glass filter placed before the detector. The filter blocked wavelengths shorter than 500 nm. The excitation channel included a 455 nm M455F1 fibre-coupled LED, collimator, LA1027-A plano-convex lens (Thorlabs, Inc. USA), diffuser and MD480 dichroic filter (Thorlabs, Inc. USA). The linear field of view of the system was 3 × 2.3 mm (height × width) at working distance 34 mm.

2.4 Data analysis and statistics

Data and statistical analysis were performed using OriginPro software (OriginLab Corp., Northampton, USA). Data are presented as a box–whisker diagram. In each box, the central line is the median, while the edges are the 25th and 75th percentiles. The differences were considered significantly different if $p < 0.05$ by a non-parametric Kruskal–Wallis test.

3 Results and discussion

Fig. 2 shows the results of the measurements using the polarographic method using the Oxytherm+R respirometer. As can be seen from the results, laser exposure with wavelengths of 1267 and 1064 nm leads to a more significant decrease in the dissolved oxygen level in the measuring chamber with the L-histidine chemical trap compared to experiments with control lasers at 1244 and 1122 nm (Fig. 2).

However, despite the shown differences between the main and reference lasers, this approach is characterised by insufficient sensitivity to the detection of various doses of generated $^1O_2$. In addition, the high sensitivity of the Clark electrode to temperature fluctuations,[42] despite the temperature stabilisation in the measuring chamber, does not allow one to analyse the change in the signal during laser exposure. Therefore, only an indirect estimate can be made after calculating the final oxygen concentration decrease compared with its initial level before exposure.

Fig. 3 shows the results of the SOSG fluorescence measurements. As can be seen from the data presented in Fig. 3, at the moment of exposure to a laser with wavelengths of 1267 nm and 1064 nm (dose of laser of 200 J cm^{-2}, 551 mW cm^{-2} power density), an increase in SOSG fluorescence is observed, which indicates $^1O_2$ production. A similar signal growth occurs under laser irradiation at a wavelength of 1244 nm. This result may indicate the production of $^1O_2$ and the incorrect use of a laser

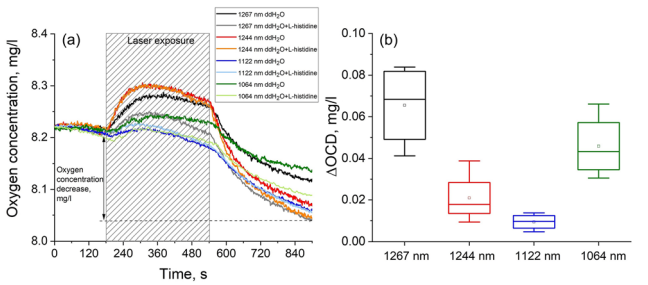

Fig. 2 Results of application of the polarographic method with Oxytherm+R respirometer at laser dose of 200 J cm^{-2}, power of 50 mW (551 mW cm^{-2} power density), 4 repetitions for each wavelength in ddH_2O or 5 mM L-histidine solution (32 measurements): (a) representative trace of kinetic changes in oxygen concentration while being illuminated with different laser sources; (b) difference in oxygen level decrease with L-histidine and without. ΔOCD was calculated as the difference between oxygen concentration decrease values with L-histidine and without.

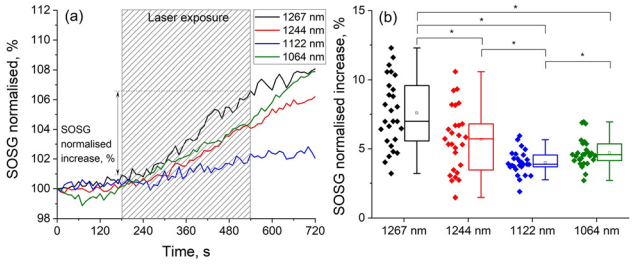

Fig. 3 Results of application of method with SOSG fluorescence intensity measurements at the dose of laser of 200 J cm^{-2}, power of 50 mW (551 mW cm^{-2} power density) (3 repetitions for each wavelength (12 measurements), 8 regions of interest in each repetition): (a) representative trace of kinetic changes in SOSG fluorescence while being illuminated with different laser sources; (b) SOSG normalised increase.

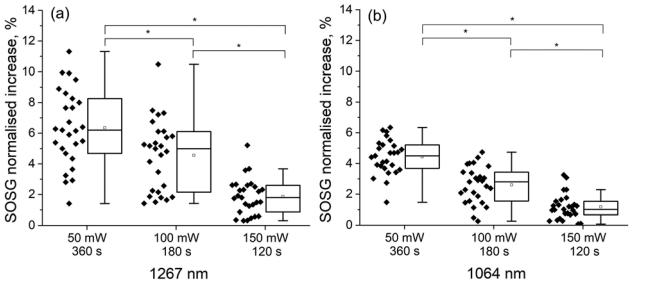

Fig. 5 Results of application of method with SOSG fluorescence intensity measurements at a 200 J cm^{-2} dose of (a) 1267 nm and (b) 1064 nm lasers for different powers of 50 mW (551 mW cm^{-2} power density, 360 s exposure time), 100 mW (1102 mW cm^{-2}, 180 s), 150 mW (1653 mW cm^{-2}, 120 s) (3 repetitions for each wavelength (9 measurements), 8 regions of interest in each repetition).

with a wavelength of 1244 nm as a reference, in contrast to a laser with a wavelength of 1122 nm, which definitely did not produce $^1O_2$. The revealed differences in an increase of SOSG fluorescence between these lasers are due to the fact that oxygen has a lower absorption coefficient on a wavelength 1122 nm, which is confirmed by the data presented in Fig. 1. Thus, the energy of light quantum is insufficient for the transition of $^3O_2$ to a singlet state.

Fig. 4 presents the results of the application of the method with SOSG fluorescence intensity measurements for lasers with wavelengths of 1267 nm and 1064 nm at 50 J cm^{-2}, 100 J cm^{-2}, 150 J cm^{-2}, 200 J cm^{-2}, 250 J cm^{-2} doses and 50 mW laser power (551 mW cm^{-2} power density). Exposure times of 90, 180, 270, 360 and 450 s were used to achieve these doses, respectively. As can be seen, the increase in SOSG fluorescence when exposed to a laser with a wavelength of 1064 nm is lower compared to a laser with a wavelength of 1267 nm, which is associated with lower absorbing properties of oxygen at a wavelength of 1064 nm.[1,43]

Estimation of the dependence of the change in the generated $^1O_2$ on the ratio of power and exposure time (the dose of 200 J cm^{-2} was the same for each power level and, while maintaining the same irradiation area, was modelled with different exposure time), in accordance with Fig. 5, indicates a greater influence on the amount of produced $^1O_2$ by the factor of exposure time rather than power. This is most likely due to the short lifetime of the generated $^1O_2$.

Fig. 6 shows the results of SOSG fluorescence intensity measurements obtained for acute brain slices before and after laser exposure. As can be seen, all three lasers show similar trends.

The basal increase in the fluorescence intensity is the result of SOSG interaction with endogenous $^1O_2$ generated by the mechanisms other than associated with irradiation.[44,45] Subsequent signal stability change may be the result of the following reasons. In the case of the 1267 nm laser, the absence of fluorescence intensity increase which was expected in accordance with the ability to generate $^1O_2$ may be explained by the significantly more complex composition of the brain slices compared to the previously used model objects, which were aqueous solutions. In slices, the generated $^1O_2$, which has a short lifetime, can participate in many alternative interactions with a higher rate due to a significant reaction constant rate and relatively low SOSG concentration. These inter-

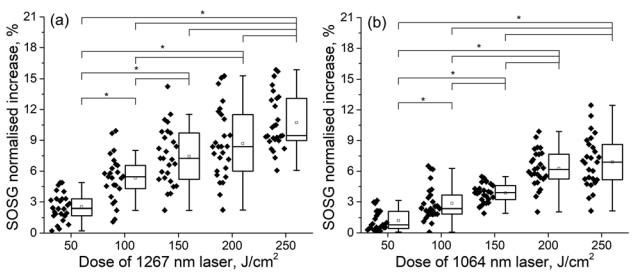

Fig. 4 Results of application of method with SOSG fluorescence intensity measurements at different doses of (a) 1267 nm and (b) 1064 nm lasers: 50 J cm^{-2}, 100 J cm^{-2}, 150 J cm^{-2}, 200 J cm^{-2}, 250 J cm^{-2}, power of 50 mW (551 mW cm^{-2} power density) (3 repetitions for each wavelength (30 measurements), 8 regions of interest in each repetition). Dose changes are provided by changing the exposure time.

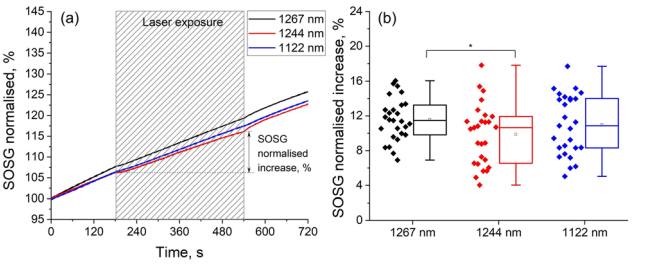

Fig. 6 Results of SOSG fluorescence intensity measurements of acute brain slices at the dose of laser of 200 J cm^{-2}, 551 mW cm^{-2} power density (3 repetitions for each wavelength (9 measurements), 8 regions of interest in each repetition): (a) representative trace of kinetic changes in SOSG fluorescence while being illuminated with different laser sources; (b) SOSG normalised increase. The selected regions were the same size and evenly distributed over the field of view for each repetition.

actions reduce or eliminate $^1O_2$ reaction with SOSG, which is necessary to form a fluorescent product. Therefore, the signal increase is based on SOSG oxidation mainly by the endogenous $^1O_2$, like the case of the 1244 nm and 1122 nm lasers. The results obtained indicate the high reactivity of $^1O_2$ in real biological systems as well as the low sensitivity of this approach when conducting studies on brain slices and the impossibility of using it in *in vivo* studies.

This work presents the results of estimating the influence of the parameters of optical systems (wavelength, power density and exposure of laser irradiation) on the generation of $^1O_2$ by instrumental methods with a chemical trap or $^1O_2$-selective fluorescent probe. These approaches differ in their sensitivity to the detection of $^1O_2$. Although they implement only an indirect estimate of the $^1O_2$ formed in the solution, these methods have shown sensitivity in detecting laser-induced $^1O_2$ at wavelengths that characterise different absorbing properties of oxygen. In addition, the use of $^1O_2$-selective fluorescent probe SOSG made to establish that the efficiency of $^1O_2$ generation relies more on the laser exposure time rather than the power. This is probably due to the short lifetime of $^1O_2$.

Undoubtedly, for *ex vivo* and *in vivo* applications, these methods have obvious limitations, and further efforts should be directed to the development of new approaches for determining the concentration of the resulting $^1O_2$. The application of the direct approach in measuring the amount of $^1O_2$ based on the detection of its luminescence at 1270 nm using highly sensitive detectors, including single photon counting, seems promising.[46,47] This approach makes it possible to determine the amount of $^1O_2$ returned to the triplet state. However, in the course of conducting methodological studies aimed at finding the optimal $^1O_2$ generation modes, it is important to determine the total amount of this ROS (reacted and returned to the triplet state $^1O_2$). To solve this task, it seems promising to use this direct method and the instrumental method with a $^1O_2$-selective fluorescent probe, which implements the estimate of $^1O_2$ that has entered into the reaction.

In conclusion, it is important to note that the heating of the medium could influence the results obtained. However, the water absorption coefficients for the wavelengths of 1267, 1244, 1122 and 1064 nm are 0.98, 0.88, 0.52 and 0.12 cm^{-1}, respectively.[48] The results show that there is no correlation between these values and the associated heating with the observed effects. In addition, our previous modelling showed the absence of significant heating of the water medium at selected radiation powers for a wavelength of 1064 nm.[49]

4 Conclusions

Although various studies reporting the initiation of apoptosis or optimisation of mitochondrial respiration by laser illumination in various types of cells and tissues have been published, there is still a knowledge gap and an essential need to identify the exact mechanism by which laser irradiation leads to these effects. Undoubtedly, further efforts should also be directed at reducing the uncertainty in the applied doses and wavelengths, developing systems to detect the concentration of produced $^1O_2$, *etc*. The mode of irradiation may also influence $^1O_2$ generation. CW or pulsed modes will contribute to various penetration of photons into the tissues and lead to different heating.[50] Although this factor can significantly affect the generation of singlet oxygen, it was not evaluated in this work.

Our study demonstrated the high efficiency of 1064 nm for generating $^1O_2$, making it possible to use this wavelength for redox biology studies. For *in vivo* studies, it may be even more effective than 1267 nm, considering the lower absorbing properties of water in this range. This will avoid heating the tissues and allow radiation to penetrate to a greater depth. Based on these results, studying the efficiency of wavelengths of 760 nm and 577 nm for $^1O_2$ generation is also interesting.

The shown increase in the concentration of singlet oxygen by increasing the exposure time makes it possible to reduce the radiation power and thus also eliminates possible thermal effects.

Data availability

Data available on request from the authors.

Author contributions

Conceptualisation: Dremin, V., Makovik, I., Vinokurov, A., Rafailov, E.; investigation: Makovik, I., Vinokurov, A.; data analysis: Makovik, I., Vinokurov, A., Dremin, V.; writing – original draft preparation: Makovik, I., Vinokurov, A.; writing – review and editing: Dremin, V., Dunaev, A., Rafailov, E.; supervision: Dremin, V., Dunaev A., Rafailov, E.; project administration: Dremin, V. All authors have given approval to the final version of the manuscript.

Conflicts of interest

There are no conflicts to declare.

Acknowledgements

The study was supported by the Russian Science Foundation under the project no. 22-75-10088.

References

1 A. Blázquez-Castro, *Redox Biol.*, 2017, **13**, 39–59.
2 V. Dremin, O. Semyachkina-Glushkovskaya and E. Rafailov, *IEEE J. Sel. Top. Quantum Electron.*, 2023, **29**, 7200911.
3 S. Zhuang, J. Demirs and I. Kochevar, *Oncogene*, 2001, **20**, 6764–6776.

4 C. Schweitzer and R. Schmidt, *Chem. Rev.*, 2003, **103**, 1685–1757.
5 S. G. Sokolovski, S. A. Zolotovskaya, A. Goltsov, C. Pourreyron, A. P. South and E. U. Rafailov, *Sci. Rep.*, 2013, **3**, 3484.
6 D. Dolgova, T. Abakumova, T. Gening, L. Poludnyakova, I. Zolotovskii, D. Stoliarov, A. Fotiadi, A. Khokhlova, E. Rafailov and S. Sokolovski, *Biomed. Opt. Express*, 2019, **10**, 4261–4275.
7 S. G. Sokolovski, E. U. Rafailov, A. Y. Abramov and P. R. Angelova, *Free Radicals Biol. Med.*, 2021, **163**, 306–313.
8 D. Dolmans, D. Fukumura and R. Jain, *Nat. Rev. Cancer*, 2003, **3**, 380–387.
9 T. Maisch, J. Baier, B. Franz, M. Maier, M. Landthaler, R. Szeimies and W. Bäumler, *Proc. Natl. Acad. Sci. U. S. A.*, 2007, **104**, 7223–7228.
10 Z. Zhou, J. Song, L. Nie and X. Chen, *Chem. Soc. Rev.*, 2016, **45**, 6597–6626.
11 D. Kurakina, A. Khilov, M. Shakhova, N. Orlinskaya, E. Sergeeva, A. Meller, I. Turchin and M. Kirillin, *J. Biomed. Opt.*, 2019, **25**, 1–17.
12 F. Borgia, R. Giuffrida, E. Caradonna, M. Vaccaro, F. Guarneri and S. Cannavò, *Biomedicines*, 2018, **6**, 12.
13 G. Gunaydin, M. Gedik and S. Ayan, *Front. Chem.*, 2021, **9**, 691697.
14 T. Zhu, M. Kim, X. Liang, J. Finlay and T. Busch, *Photonics Lasers Med.*, 2015, **4**, 59–71.
15 J. Skovsen, E. Snyder, J. Lambert and P. Ogilby, *J. Phys. Chem. B*, 2005, **109**, 8570–8573.
16 S. Hatz, J. Lambert and P. Ogilby, *Photochem. Photobiol. Sci.*, 2007, **6**, 1106–1116.
17 P. Merkel and D. Kearns, *J. Am. Chem. Soc.*, 1972, **94**, 7244–7253.
18 I. N. Novikova, E. V. Potapova, V. V. Dremin, A. V. Dunaev and A. Y. Abramov, *Life Sci.*, 2022, **304**, 120720.
19 O. Semyachkina-Glushkovskaya, S. Sokolovski, A. Goltsov, A. Gekaluyk, E. Saranceva, O. Bragina, V. Tuchin and E. Rafailov, *Prog. Quantum Electron.*, 2017, **55**, 112–128.
20 H. Wu, Q. Song, G. Ran, X. Lu and B. Xu, *TrAC, Trends Anal. Chem.*, 2011, **30**, 133–141.
21 E. Koh and R. Fluhr, *Plant Signaling Behav.*, 2016, **11**, e1192742.
22 B. Li, L. Lin, H. Lin and B. Wilson, *J. Biophotonics*, 2016, **9**, 1314–1325.
23 E. Hideg, C. Spetea and I. Vass, *Photosynth. Res.*, 1994, **39**, 191–199.
24 G. Nardi, I. Manet, S. Monti, M. Miranda and V. Lhiaubet-Vallet, *Free Radicals Biol. Med.*, 2014, **77**, 64–70.
25 M. Ruzzi, E. Sartori, A. Moscatelli, I. Khudyakov and N. Turro, *J. Phys. Chem. A*, 2013, **117**, 5232–5240.
26 M. Jarvi, M. Patterson and B. Wilson, *Biophys. J.*, 2012, **102**, 661–671.
27 A. Jiménez-Banzo, S. Nonell, J. Hofkens and C. Flors, *Biophys. J.*, 2008, **94**, 168–172.
28 A. Telfer, S. M. Bishop, D. Phillips and J. Barber, *J. Biol. Chem.*, 1994, **269**, 13244–13253.
29 Y. Nosaka and A. Y. Nosaka, *Chem. Rev.*, 2017, **117**, 11302–11336.
30 X. Ragàs, A. Jiménez-Banzo, D. Sánchez-García, X. Batllori and S. Nonell, *Chem. Commun.*, 2009, 2920–2922.
31 F. Anquez, A. Sivéry, I. E. Yazidi-Belkoura, J. Zemmouri, P. Suret, S. Randoux and E. Courtade, *Singlet Oxygen: Applications in Biosciences and Nanosciences*, 2016, pp. 75–91.
32 G. Gurinovich, *J. Appl. Spectrosc.*, 1991, **54**, 243–249.
33 F. Anquez, I. Yazidi Belkoura, P. Suret, S. Randoux and E. Courtade, *Laser Phys.*, 2013, **23**, 025601.
34 P. Ogilby, *Chem. Soc. Rev.*, 2010, **39**, 3181–3209.
35 A. Krasnovsky Jr., *Phys. Wave Phenom.*, 2020, **28**, 116–134.
36 C. Flors, M. Fryer, J. Waring, B. Reeder, U. Bechtold, P. Mullineaux, S. Nonell, M. Wilson and N. Baker, *J. Exp. Bot.*, 2006, **57**, 1725–1734.
37 S. Kim, M. Fujitsuka and T. Majima, *J. Phys. Chem. B*, 2013, **117**, 13985–13992.
38 X. Cheng, A. Vinokurov, E. Zherebtsov, O. Stelmashchuk, P. Angelova, N. Esteras and A. Abramov, *J. Neurochem.*, 2021, **157**, 1234–1243.
39 A. Vinokurov, V. Dremin, G. Piavchenko, O. Stelmashchuk, P. Angelova and A. Abramov, *Assessment of Mitochondrial Membrane Potential and NADH Redox State in Acute Brain Slices*, Springer US, New York, NY, 2021, pp. 193–202.
40 A. Gollmer, J. Arnbjerg, F. Blaikie, B. Pedersen, T. Breitenbach, K. Daasbjerg, M. Glasius and P. Ogilby, *Photochem. Photobiol.*, 2011, **87**, 671–679.
41 I. Novikova, A. Manole, E. Zherebtsov, D. Stavtsev, M. Vukolova, A. Dunaev, P. Angelova and A. Abramov, *Free Radicals Biol. Med.*, 2020, **159**, 15–22.
42 M. Miniaev, M. Belyakova, N. Kostiuk, D. Leshchenko and T. Fedotova, *J. Anal. Methods Chem.*, 2013, **2013**, 249752.
43 A. Kozlov, O. Egorova, O. Medvedkov and A. Krasnovsky, *Opt. Lett.*, 2021, **46**, 556–559.
44 K. Murotomi, A. Umeno, M. Shichiri, M. Tanito and Y. Yoshida, *Int. J. Mol. Sci.*, 2023, **24**, 2739.
45 A. Onyango, *Oxid. Med. Cell. Longevity*, 2016, **2016**, 2398573.
46 A. Moskalensky, T. Karogodina, A. Vorobev and S. Sokolovski, *HardwareX*, 2021, **10**, e00224.
47 N. Gemmell, A. McCarthy, B. Liu, M. Tanner, S. Dorenbos, V. Zwiller, M. Patterson, G. Buller, B. Wilson and R. Hadfield, *Opt. Express*, 2013, **21**, 5005–5013.
48 G. M. Hale and M. R. Querry, *Appl. Opt.*, 1973, **12**, 555–563.
49 V. Dremin, I. Novikova and E. Rafailov, *Opt. Express*, 2022, **30**, 23078–23089.
50 D. Galiakhmetova, V. Dremin, A. Koviarov, D. Stoliarov, N. Ngum, R. C. Murugesan, R. Parri, S. Sokolovski and E. U. Rafailov, *IEEE J. Sel. Top. Quantum Electron.*, 2023, **29**, 7200311.